High-pressure single-mode CO_2 laser with picosecond plasma shutter

Joachim Knittel
Damien P. Scherrer
Fritz K. Kneubühl
Swiss Federal Institute of Technology
Institute of Quantum Electronics, ETH
Infrared Physics Laboratory
CH-8093 Zurich, Switzerland

Abstract. The authors describe the realization of a single-longitudinal-mode high-pressure CO_2 laser with a plasma shutter. Single-mode operation is achieved with a three-mirror resonator with etalon. The resonator includes a subcavity, which protects the temperature-controlled etalon from destruction by high radiation intensities. In particular we have investigated two subcavity configurations, which use different etalons and grating arrangements. The maximal pulse energy of about 140 mJ was achieved with a grating that is employed in grazing incidence. A theoretical model has been developed, which illustrates the nonlinear frequency-tuning behavior of the three-mirror resonator and explains how the subcavity has to be adjusted to optimize the mode discrimination of the resonator. With the help of a plasma shutter we have produced tunable truncated 10-μm laser pulses. These pulses were employed to generate 100-ps pulses by optical free induction decay (OFID). With our system we produced for the first time OFID pulses 15 GHz off a CO_2 laser line center and investigated the effects of a frequency detuning between the laser frequency and the absorption line of the spectral filter in an OFID system.

Subject terms: CO_2 laser; optical free induction decay (OFID); three-mirror resonator; subcavity; far-infrared (FIR) pulses.

Optical Engineering 34(7), 2000–2016 (July 1995).

1 Introduction

High-pressure CO_2 lasers, which work in the mid infrared, were developed in the seventies.[1,2] The particularity of this type of laser is the high laser-gas pressure, which lies between 10 and 20 bar. Pressure broadening causes an overlap of neighboring laser transitions. Thus a large amplification bandwidth is achieved. This bandwidth makes the laser continuously tunable within large regions of the 9.4- and 10.4-μm bands of the CO_2 laser gas. Furthermore, the high pressure reduces the gain rise time, which varies inversely with the pressure.[3] Gain-switched pulses with intensities over 50 MW/cm^2 are easily obtained.[4] The combination of high output power and large amplification bandwidth makes this laser type attractive for short-pulse generation by mode locking,[5,6] for amplifying ultrashort infrared pulses,[7,8] and as a pump source for mid- and far-infrared (FIR) lasers.[9,10]

By reducing the bandwidth to a single longitudinal mode, smooth pulses with a bandwidth of less than 100 MHz are produced. Such a laser is especially interesting as a tunable radiation source for molecular spectroscopy, for remote sensing of the atmosphere,[11] and for optical pumping of FIR lasers. A monochromatic pump source is capable of higher pumping efficiencies than a free-running laser,[12] as well as able to induce new submillimeter transitions to oscillate, which are not observed with a multimode laser. Optically pumped FIR lasers would achieve drastically enhanced FIR power and better frequency tunability.[13] Although considerable work has been performed to develop resonator configurations that achieve single-mode operation with this type of laser, an ideal method has not been found hitherto.[14]

In general, single-mode operation is achieved by keeping the gain for all but the desired mode below the laser threshold. This can be achieved by introducing frequency-dependent losses in the resonator or by increasing the gain of one mode with an additional laser.[15]

For the well-known transversely excited atmospheric pressure (TEA) CO_2 laser, which is similar to the high-pressure CO_2 laser but operates at atmospheric pressure,[16] methods to achieve single-mode operation are well developed. These laser systems are routinely used for many different applications. Comprehensive reviews were published by Chin[17] and Quack et al.[18] However, with high-pressure CO_2 lasers single-mode operation is harder to achieve. Their gain bandwidth is several hundred gigahertz wide, compared to the 4-GHz bandwidth of a TEA CO_2 laser, and therefore mode discrimination techniques have to be effective over a much wider spectral range. Furthermore, all optical elements introduced into the resonator have to be protected against the high power density inside the resonator. Nevertheless, most of the methods developed so far are quite similar to those applied in TEA lasers.

Two common ways to achieve single-mode operation with TEA lasers make use of an absorber gas cell in the resonator[18]

Paper SWI-40 received Nov. 7, 1994; revised manuscript received Jan. 17, 1995; accepted for publication Jan. 26, 1995.

or a CO_2 hybrid laser, which is a combination of a TEA laser with a low-pressure gain section.[19] Since these two principles allow only limited tunability, they are not interesting for a continuously tunable system.

The application of intracavity etalons is a well-established method with TEA CO_2 lasers.[17,11] However, in a high-pressure CO_2 laser only low-finesse etalons, which do not permit single-mode operation,[20] can be directly introduced in the resonator. An etalon with a sufficiently high finesse would be immediately destroyed by the high field intensities in the cavity. This problem can be reduced by the use of a three-mirror resonator.

The basic three-mirror resonator consists of a grating, a partially reflective mirror, and an output coupler. With this resonator type, single-mode operation is only achieved with short resonator lengths and by operation near threshold. Therefore only low pulse energies are possible. Thus Deka et al.[21] obtained about 20 mJ per pulse with a cavity length of 0.4 m.

By introducing an etalon in the three-mirror resonator at the position shown in Fig. 1(a), better mode separation is achieved and longer cavities can be used. As we demonstrate later, the intensity passing through the etalon is considerably reduced in this arrangement. With such a resonator Deka et al.[22] achieved pulse energies up to 150 mJ. The advantages of this resonator are its simple optical adjustment, the compact setup, the easy availability of its optical components, and the possibility of achieving high pulse energies. A modification of the three-mirror resonator is shown in Fig. 1(b).[23] Here, the grating is used in grazing incidence, which increases its frequency selectivity. A major disadvantage of the three-mirror resonator is its complicated frequency-tuning behavior, which is caused by the mutual influence of the bandwidth-limiting elements within the resonator. This resonator type has been theoretically investigated by Botha et al.,[14] who discussed certain aspects of its mode discrimination properties and its frequency stability. Nevertheless, there are still unsolved problems such as the detailed frequency tuning behavior and criteria to achieve optimal mode discrimination. Some of these questions are discussed in this study.

The use of a so-called modified Fabry-Perot (MFP) interferometer as a frequency-dependent output coupler offers an attractive alternative to the three-mirror resonator. The setup, which is shown in Fig. 1(c), is successfully employed in TEA CO_2 lasers.[24,25] By introducing a low-finesse etalon with a large free spectral range (FSR) of 20 GHz into the resonator, Kovar et al.[26] obtained single-mode operation with a high-pressure CO_2 laser. By varying the mirror spacing of the MFP, fine frequency tuning over a range of about 2 GHz was achieved. However, the etalon was slightly damaged during the experiments, and the optical alignment of the cavity proved to be quite difficult.

The principle of injection locking, whose schematic setup is shown in Fig. 1(d), consists of selectivity amplifying a single mode. An external laser beam is injected into the main cavity. Laser oscillation occurs at the axial mode nearest the injected frequency and not at the frequency of the injected signal.[27] Because no optical components are needed within the resonator, high pulse intensities can be generated. By injection locking with a nontunable cw CO_2 laser, single-mode pulses with pulse energies up to 180 mJ were reported by Chandonnet et al.[28] The required intensity of the injected

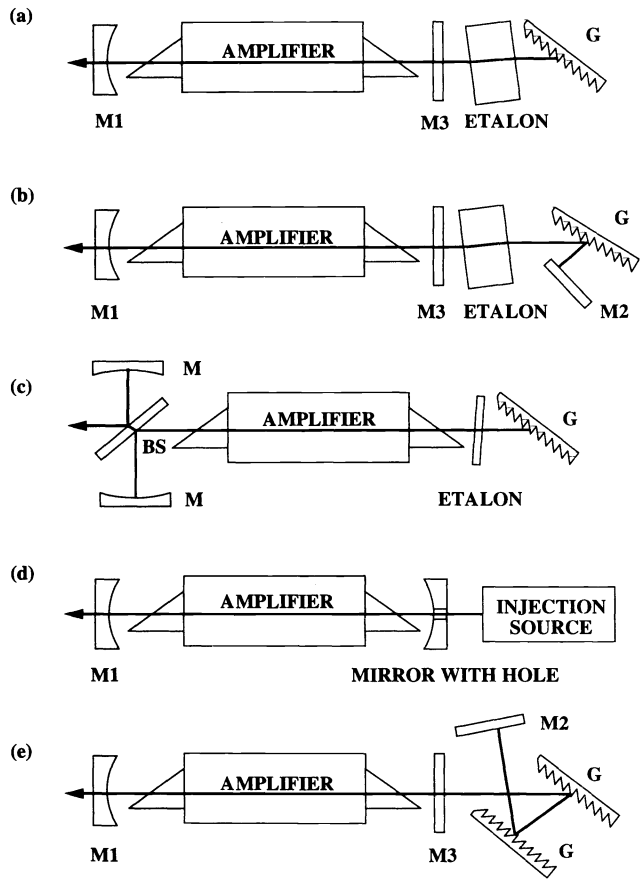

Fig. 1 Resonator types that permit single-longitudinal-mode operation with a high-pressure CO_2 laser: (a) three-mirror resonator with an etalon; (b) resonator similar to (a), but with a grating in grazing incidence; (c) modified Fabry-Perot interferometer; (d) injection locking; (e) two-grating resonator: outcoupling mirror M1, plane mirror M2, partially reflective mirror M3, grating G, and beamsplitter BS.

radiation is about 1 mW/cm^2 for cw sources and 20 kW/cm^2 for 50-ns pulses.[4] In order to allow tunability, a tunable injection source is obviously needed. To our knowledge the use of such a source has not yet been reported. This is probably due to the lack of suitable injection sources. One possible injection source is a $Pb_{1-x}Sn_xTe$ diode laser, but there occur problems with stray radiation, which is reinjected from the main laser back into the diode laser.[4] Nevertheless, injection locking is a promising scheme, since single-mode pulse energies over 300 mJ are possible.

Recently, Izatt et al.[29] proposed the use of a two-grating resonator for single-mode operation. The suggested setup is shown in Fig. 1(e). The great advantage of this resonator is that frequency tuning over a wide range is possible simply by tuning one of the gratings. However, specially manufactured gratings with large blaze angles are needed to limit the losses at the large angles of incidence, which are necessary to achieve sufficient spectral resolution. Until now this scheme has worked successfully only with TEA lasers.[29] A system using a high-pressure CO_2 laser is under construction.[30]

A summary of the characteristics of the four most important experimental arrangements to achieve single-mode operation with high-pressure CO_2 lasers is presented in Table 1.

Table 1 Review of single-mode high-pressure CO_2 lasers.

resonator type	main advantages	main disadvantages	max. pulse energy	references remarks
3-mirror resonator with etalon	simple optical adjustment only standard optical components needed	complicated tuning behaviour	150 mJ	[22,23,35]
reflective multipass interferometer	long resonator cavities possible	difficult optical alignment damage of optics	180 mJ	[26]
injection locking	highest possible pulse energy no opt. components within the cavity	tunable injection source needed	> 300 mJ	[4,28] (both with non-tunable injection source)
two-grating resonator	simple frequency tuning behaviour	specially manufactured gratings needed		[29,30] (not yet realized)

Our interest in single-mode high-pressure CO_2 lasers is focused on the production of frequency-tunable truncated laser pulses. Truncated pulses are generated by interrupting a smooth laser pulse with a plasma shutter. Truncation times down to 10 ps are achieved. These pulses are well suited for producing ultrashort pulses in the 10-μm range by optical free induction decay (OFID)[31] and for the generation of short superradiant pulses in the FIR region.[32] Until now all these systems have worked with hybrid TEA CO_2 lasers, which operate only on the discrete vibration-rotational lines of the CO_2 gas. This drastically reduces the number of available pump lines in FIR gases, which are used as spectral filters for the OFID systems[32] and for generating superradiant pulses, as they have to coincide with the lines of the laser. In order to become independent of these random coincidences, we have constructed a continuously tunable single-mode high-pressure CO_2 laser and combined it with a plasma shutter.

For the single-mode laser, we have chosen a three-mirror resonator with etalon. Because the laser frequency is kept fixed during our experiments, the nonlinear frequency-tuning characteristics of this resonator are not a disadvantage. With this system we have produced tunable truncated CO_2 laser pulses, which we used to generate 100-ps mid-infrared pulses by OFID and single superradiant FIR pulses. This is the topic of Sec. 4. First, we give a detailed theoretical and experimental description of our high-pressure single-mode CO_2 laser system in Secs. 2 and 3.

2 Theoretical Analysis of the Three-Mirror Resonator

2.1 *A Model of the Three-Mirror Resonator*

As mentioned in the introduction, the three-mirror resonator with etalon shows a nonlinear and quite complicated frequency-tuning characteristic, which is due to the combined influence of etalon, grating, and mirrors. We recently gave a simple intuitive explanation for this nonlinear behavior.[23] Here, we present a more accurate model. The aim of the model is to understand the tuning behavior qualitatively and to find criteria to optimize the performance of this resonator. In the following investigation, we refer to the three-mirror resonator shown in Fig. 1(b). The results can easily be adapted to the resonator presented in Fig. 1(a).

The resonator consists principally of an outcoupling mirror M1 and a subcavity. The subcavity, whose optical components are shown in Fig. 2, can be considered as a mirror with a frequency-dependent reflectivity $R(\nu)$. The two mirrors form a Fabry-Perot resonator, which we call the main cavity. The main cavity is responsible for a discrete longitudinal-mode spacing of about 120 MHz for a typical cavity length of 1.25 m. The mode spacing depends on the cavity length. It is slightly modified by phase shifts caused by the subcavity. In order to select a single longitudinal mode, the main-cavity length has to be readjusted for each new frequency, so that the maximum of the subcavity reflectivity $R(\nu)$ coincides with one of these discrete longitudinal modes. If this condition is not fulfilled, the laser runs simultaneously in two modes. This implies that the subcavity alone determines the laser frequency within at most ± 60 MHz. This accuracy is sufficient for our purposes. Consequently, we neglect the influence of the main resonator as well as the phase of $R(\nu)$.

In the following we show calculations of the reflectivity $R(\nu)$ by taking into account multiple reflections in the subcavity. Our model is similar to that presented by Botha et al.[14] However, we always employ complex numbers to keep track of the phase shifts within the subcavity. This is important, because the phase shifts generated by the etalon narrow the peaks of $R(\nu)$. To simplify the calculation we have approximated all electromagnetic waves by plane waves and neglected phase shifts introduced by the grating. The schema and parameters of the calculation are presented in Fig. 2. Intensity reflection and transmission coefficients are always written in uppercase, whereas amplitude factors are written in lowercase. For single-longitudinal-mode operation the function $R(\nu)$ requires a reflection maximum that is sufficiently higher than all other maxima and has a sufficiently small width for the selection of a single mode.

The reflectivity r_g of the grating as a function of the frequency ν can be approximated by a Gauss function[29]:

$$r_g = R_{\max}^{1/2} \exp\left[-(2\ \ln 2)\left(\frac{\nu-\nu_0}{\Delta\nu_g}\right)^2 \right] . \tag{1}$$

The parameter $R_{\max}$ indicates the maximal reflectivity of the grating at the frequency $\nu=\nu_0$. The half-width $\Delta\nu_g$ of the grating can be approximately calculated if the beam divergence within the resonator is known.[33] For our experimental setup we obtained $\Delta\nu_g \approx 9$ GHz for a grating with 150 lines/mm at a grazing-incidence angle of 60 deg.

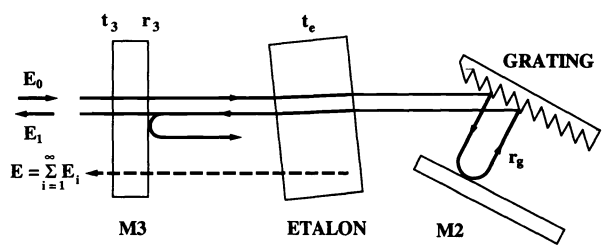

Fig. 2 Schematic of a subcavity consisting of a partially reflective mirror M3, an etalon, a grating G, and a plane mirror M2. This schematic is used for the calculation of the total subcavity reflectivity $R(\nu)$.

The transmission coefficient t_e of the etalon is given by[34]

$$t_e = \frac{t^2 a \exp[-i(k-k_0)l]}{1-r^2a^2 \exp[-2i(k-k_0)l]} \quad \text{with}$$

$$k = \frac{2\pi}{c}\nu \text{ and } l = n_{et} l_{et} , \tag{2}$$

where

t = amplitude transmission of the coating
r = amplitude reflection of the coating
a = transmission per pass due to absorption losses
c = speed of light
k_0 = offset, which is used to shift position of transmission peaks
n_{et} = index of refraction
l_{et} = length of the etalon.

The parameter k_0 is introduced in Eq. (2) to shift the frequency of the transmission peaks of the etalon. In the experiment this shift is introduced by changing the temperature-dependent refractive index $n_{et}(T)$ of the etalon. It can be shown that for small changes of n_{et}, the effect of changing k_0 is equivalent to changing n_{et}.

The total reflected amplitude E_r from the subcavity is evaluated by summing all the reflections E_i from the impinging electric wave E_0 according to Fig. 2. It should be noticed that the wave passes two times over the grating per round trip in the grazing incidence arrangement. The reflectivity of the mirror M2 is set equal to one. The calculation yields the following formula:

$$E_r = E_0 \left\{ r_3 + \frac{t_3^2 t_e^2 r_g^2 \exp[2ik(L_{sub}-l_{et}]}{1+t_e^2 r_g^2 r_3 \exp[2ik(L_{sub}-l_{et})]} \right\} . \tag{3}$$

The subcavity length L_{sub} is the geometrical distance between the mirrors M2 and M3 including the reflection at the grating. As the phase shift introduced by the etalon is already incorporated in the complex factor t_e, the length of the etalon l_{et} has to be subtracted from L_{sub} in (3).

Finally, the intensity reflection R of the subcavity is determined by

$$R = \frac{E_r E_r^*}{E_0 E_0^*} . \tag{4}$$

With the help of Eqs. (1)–(4), we have calculated R as a function of the frequency. The numerical data were chosen in accordance with our experimental setup. The etalon in the subcavity had a reflectivity of 60% and a FSR of 3.1 GHz. Typical results of these calculations are shown in Fig. 3(a)–3(d).

The subcavity reflectivity R is modulated near $R_3 = 0.4$, which corresponds to the reflectivity of the mirror M3. The modulations decrease to both sides of the diagram, due to the grating. The peaks correspond to transmission maxima of the etalon, whereas the fast modulations of R are caused by multiple reflections between the mirrors M2 and M3. In Fig. 3(a) the subcavity is in antiresonance with the etalon peaks, whereas in Fig. 3(b) all the peaks are in resonance. Antiresonance means that there exists no standing wave in the subcavity. This is the preferred state, as the subcavity, which behaves like a Fabry-Perot interferometer, exhibits maximum reflectivity in antiresonance. In Fig. 3(b) appear two equal strong reflection peaks at a distance of about 400 MHz. This means that single-mode operation is not possible. The beating of these two modes has been experimentally observed after carefully adjusting L_{sub}.

In Eq. (3) we have assumed that the grating and mirrors of the subcavity are perfectly aligned. This is certainly not the case in the experiment. Therefore, the influence of the multiple reflections in the subcavity just mentioned will be less pronounced. Nevertheless, the experiments described in Sec. 3 are qualitatively in accordance with our model.

2.2 *Relevant Parameters of the Subcavity*

In this section we discuss the influence of the subcavity length L_{sub} and the reflectivity R_3 of the mirror M3 on the mode selectivity of the resonator. The mode selectivity is defined as the intensity ratio between the strongest and the second strongest modes I_1 and I_2, which correspond to the reflection maxima R_{max1} and R_{max2} of the subcavity. Here we assume that the modes I_1 and I_2 result from different reflection peaks, which are typically separated by the FSR of the etalon. Neighboring modes can be suppressed by adjusting the main-cavity length, as discussed in Sec. 2.1. Assuming a frequency-independent amplification factor, the intensity ratio of the two strongest modes I_1 and I_2 is given by[14]

$$\frac{I_1}{I_2} = \left(\frac{R_{max1}}{R_{max2}} \right)^N , \tag{5}$$

where N is the number of cavity round trips that are necessary for buildup of the laser pulse. For example, with a typical number of round trips $N = 35$ and $R_1/R_2 = 1.1$, an intensity ratio of $I_1/I_2 \approx 28$ is achieved.

First we consider the influence of the subcavity length L_{sub}. In Fig. 3, $R(\nu)$ is plotted for two different lengths L_{sub}, where case A corresponds to $L_{sub} = 16.4$ cm and case B to $L_{sub} = 18.8$ cm. Here L_{sub} is responsible for the periodicity of the fast modulations of $R(\nu)$, which were mentioned in Sec. 2.1. In case A this modulation frequency is exactly 4 times that introduced by the etalon. Therefore, the influence of the fast modulations is the same for all etalon peaks. On the contrary, the modulation frequency in case B is about 4.5 times that of the etalon, and so the transmission peaks of the etalon are alternatingly in resonance and in antiresonance with the subcavity.

The best mode selectivity is obviously achieved in Fig. 3(c). However, if the etalon peaks are shifted half a period relative to the fast modulations, the central peak is attenuated, whereas the adjacent peaks are amplified. The practical consequence is a large jump of the laser frequency, on the order of the FSR of the etalon.

Detailed tuning behavior for the two cases is shown in Fig. 4(a) and 4(b). The graphs correspond to the situations discussed in Fig. 3. As expected, there are large frequency jumps in case B [Fig. 4(b)], while there are only minor ones in case A. It should also be noticed that the mode selectivity

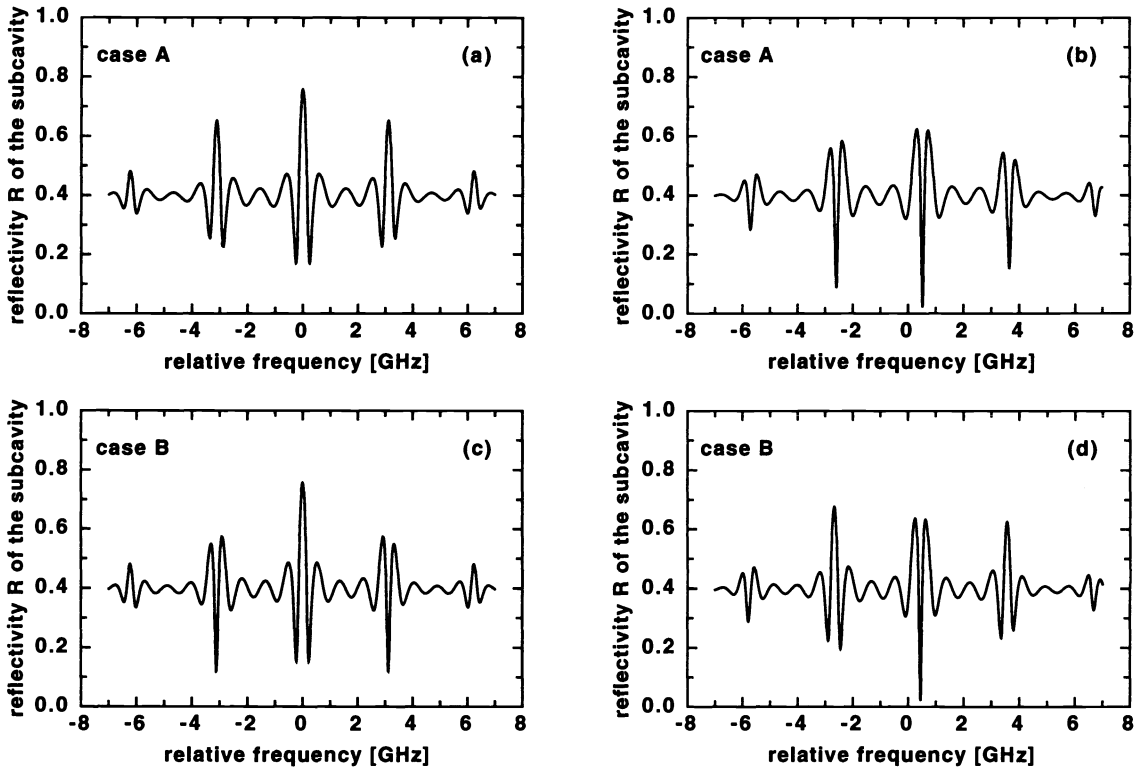

Fig. 3 Frequency-dependent reflectivity $R(\nu)$ for a subcavity length L_{sub} of 16.4 cm (case A) and 18.8 cm (case B). The zero position (0 GHz) corresponds to a wavelength of 10 μm. In (b) and (d) the position of the etalon peaks is shifted by about 440 MHz relative to the situation shown in (a) and (c).

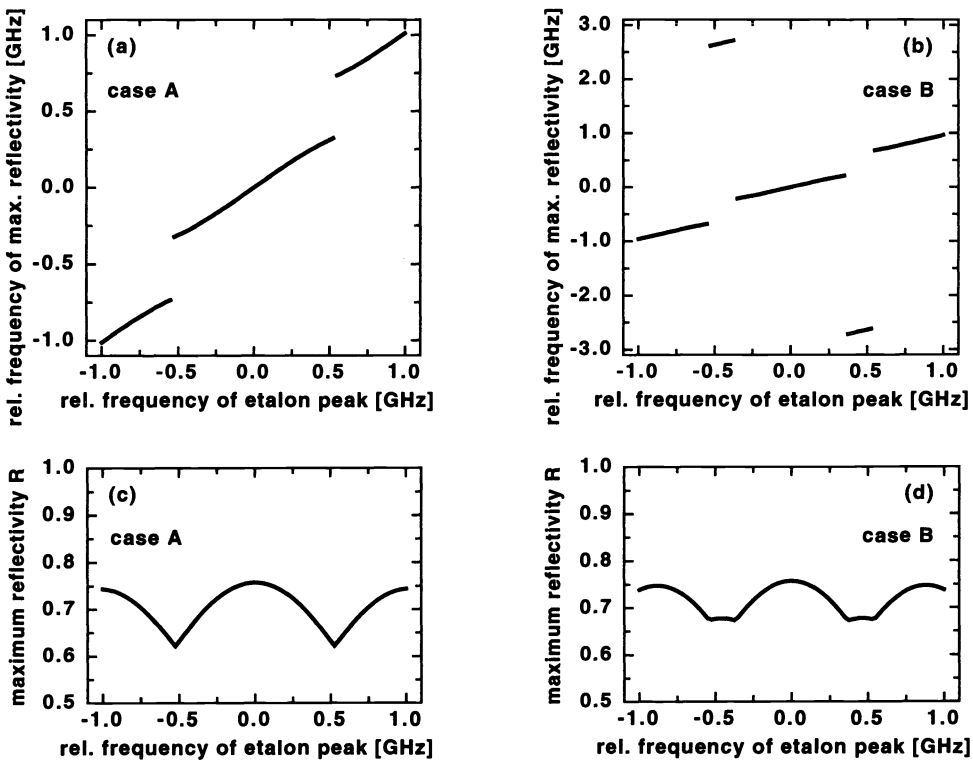

Fig. 4 (a) and (b): The relative frequency of the maximal subcavity reflectivity R plotted versus the relative frequency of the etalon transmission peaks. The subcavity length L_{sub} is 16.4 cm in case A and 18.8 cm in case B. Notice the different scales on the vertical axes. (c) and (d): Maximal reflectivity R of the subcavity as a function of the relative position of the etalon transmission peaks for both cases.

in the proximity of the frequency jumps is low, because there exist at least two reflection peaks of comparable strength.

Another important aspect is the dependence of the maximal subcavity reflection on the frequency position of the etalon peaks for the two cases cited above. This is presented in Figs. 4(c) and 4(d). In both cases the regions of minimal reflection are situated at the frequency jumps that occurred in Figs. 4(a) and 4(b). As the output power of the laser is directly correlated to the reflectivity R of the subcavity, the pulse energy is minimal close to the frequency jumps and has a maximum between.

Finally, we have investigated the influence of the reflectivity R_3 of the mirror M3 on the mode selectivity. In Fig. 5 we have plotted the maxima for the ratio I_1/I_2 as functions of the reflectivity R_3 for case A (solid line) and case B (dashed line). The special situations for $R_3 = 0.4$ are shown in the diagrams of Fig. 3(a) and 3(c). The ratio R_1/R_2 was determined numerically using these diagrams. Subsequently, the ratio I_1/I_2 was calculated with Eq. (5). The number of cavity round trips N is approximately 35 for our laser system.[8,35] Because a high value of R_3 decouples the subcavity from the main cavity, the mode selectivity drops for higher R_3. This is also true for the discrimination between neighboring modes within a reflection peak, since the influence of the etalon on the main cavity is reduced by high R_3.

2.3 *Discussion*

The theoretical investigation has demonstrated that the subcavity of the three-mirror resonator should always be operated in antiresonance. This ensures maximal output power, high mode discrimination, and the most stable output frequency. Experimentally this favorable operation region can be found by changing L_{sub} with a piezoelectric element to determine the position of maximum pulse energy of the laser. Yet the coarse length of the subcavity should be determined first, so that the laser operates as in case B, where maximal mode selectivity is achieved. This length L_{sub} (case B) is given by

$$L_{sub}(\text{case B}) = l_{et}\left[n_{et}\left(m + \frac{1}{2} \right) + 1 \right] \quad \text{with}$$

$$m = 0,\ 1,\ 2,\ 3,\ \ldots\ , \tag{6}$$

where m is typically 3 or 4.

To achieve linear tunability in a frequency range of 1 GHz the temperature of etalon and L_{sub} have to be changed simultaneously. This is only possible if the thermal drift of L_{sub} can be kept below ± 0.5 μm. For larger linear frequency scans simultaneous tuning of the grating angle is also necessary. In this case the dependence of L_{sub} on the grating position needs to be considered also. All this makes the experimental realization of a linear tunable laser system with a three-mirror resonator rather complex.

3 Design and Operation of a Single-Mode High-Pressure CO_2 Laser

3.1 *The Three-Mirror Resonator with Etalon*

The main components of our laser system, which employs a three-mirror resonator with etalon, are shown in Fig. 6. It

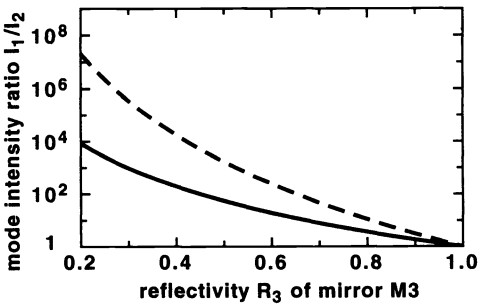

Fig. 5 Intensity ratio of the two strongest modes versus the reflectivity R_3 of mirror M3 for two subresonator lengths, case A (solid curve) and case B (dashed curve).

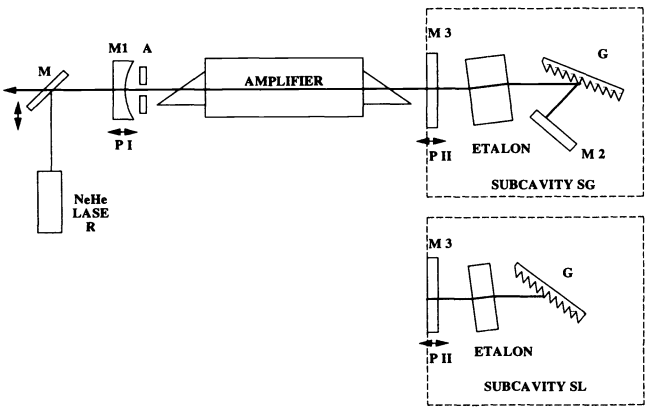

Fig. 6 The three-mirror resonator with the two investigated subcavities SG and SL includes an outcoupling mirror M1, a variable aperture A, a partial reflective plane mirror M3, a grating with 150 lines/mm, a plane gold mirror M2 and two piezoelectric elements P I and P II.

consists of a spherical outcoupling mirror M1 with a radius of 20 m and a reflectivity between 70% and 80%, a high-pressure amplifier, and a subcavity. We have examined two subcavities SG and SL, which comprehend different etalons and grating arrangements. A coarse bandwidth reduction is achieved by the grating, whereas the etalon forces the laser into a single longitudinal mode. The subcavity SG includes a grating in grazing incidence, which produces a greater bandwidth reduction than the standard Littrow arrangement in SL. Therefore, an etalon with a smaller FSR can be used in SG than in SL. The main features are summarized in Table 2. A variable aperture is introduced close to the mirror M1 to favor the TEM_{00} mode.

The introduction of the partially reflective mirror M3, which is also called the "third mirror," considerably reduces the radiation intensity in the subcavity. The intensity is reduced because the subcavity works in antiresonance, i.e., destructive interference of the laser radiation, contrary to a regular Fabry-Perot interferometer. This is necessary to protect the grating and especially the etalon from destruction. In Fig. 7 we have plotted the ratio of the intensity in the subcavity so that in the main cavity for the subcavity SG, as a function of the reflectivity R_3 of the mirror M3.[36] Thus, with a 40% reflectivity of M3 the intensity in the subcavity is only 26% of that in the main cavity. Furthermore, M3 increases the maximal reflectivity of the grating-mirror

Table 2 Specifications of the investigated subcavities.

	subcavity SG	subcavity SL
grating (150 lines/mm)	grazing incidence at 60°	Littrow
etalon (ZnSe) thickness	2 cm	1 cm
etalon reflectivity at 10.6 μm	60 %	80 %
free spectral range (FSR)	3.1 GHz	6.2 GHz
theoretical finesse F	6	14
reflectivity R_3 of mirror M3	40 %	40 or 50 % at 10 μm 40 % at 9 μm
subcavity length L_{sub}	0.14 m	0.09 m
main cavity length	1,2 m	1,15 m
output coupler reflectivity	80 % or 70 %	70 % at 10 μm 80 % at 9 μm

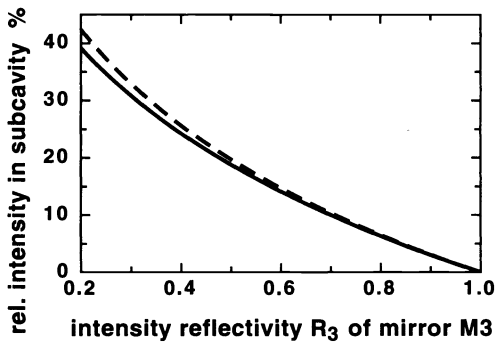

Fig. 7 Intensity in the subcavity relative to the intensity in the main cavity versus reflectivity R_3 of mirror M3 with no loss (dashed curve) and with a 15% loss per path in the subcavity (solid curve).

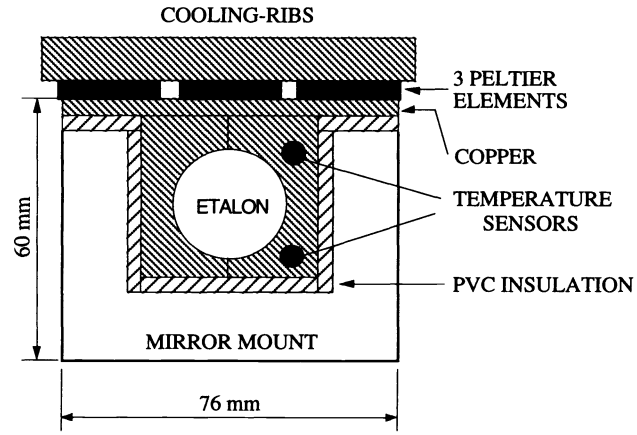

Fig. 8 Compact etalon mount, which permits temperature control of the etalon and optical adjustment in the cavity.

combination[37] and partially compensates for the dropoff in efficiency that results from the high losses due to the etalon (Sec. 3.3) and the grating at grazing incidence.[38] The subcavity length L_{sub} is kept as short as possible to avoid deformation of the Gaussian mode structure. The mirror M3 is mounted on a precision translation stage, whose length is fine-tunable with a piezoelectric element. To reduce thermal length drifts, the distance between the grating and M3 of the subcavity SG was fixed by a quartz tube, which was connected to the grating and the translation stage. Since the thermal expansion coefficient of quartz is only 0.5×10^{-6} K^{-1}, the length drift of the 9-cm-long subcavity is mainly determined by the piezoelectric element. The piezoelectric element has a thermal expansion of about 0.5 μm/K. The influence of the temperature drift on the output frequency of the laser was investigated by Botha et al.[14]

3.2 *The Etalons*

The etalons consist of ZnSe cylinders, whose coated end surfaces have a wedge of less than 1 arcsec and a flatness of better than $1/100$ at 10.6 μm. ZnSe is highly resistant to optical damage, is transparent for a visual alignment laser, and has an extremely low absorption coefficient at 10 μm. The main technical data on the two etalons are included in Table 2. Each etalon is built into a copper block, which can be incorporated into a mirror mount. The construction is shown in Fig. 8. Three Peltier elements, which are connected to a temperature controller, are used to stabilize the temperature of the etalon. A temperature-dependent resistor (Omega No. 44005, Stamford, USA) forms part of a bridge circuit. The signal from the bridge is detected with a lock-in amplifier and fed into the temperature controller.[39] The temperature is measured separately with an integrated precision centigrade temperature sensor (LM35AH). Its relative accuracy is better than ±0.05 K. The copper block guarantees fast and homogenous heat exchange between the etalon and the Peltier elements. Furthermore, the copper block, which is insulated with PVC against the mirror mount and with foam against the surroundings, serves as a heat buffer. A temperature change of 1 K shifts the transmission peaks of the etalon by about 1 GHz. This is due to the temperature-dependent length and refractive index of the ZnSe etalon.[11]

The selection of the finesse F and the FSR of the etalons is a difficult task. On the one hand, high F and FSR would be ideal to achieve stable single-mode operation. On the other hand the losses in the subcavity, which are mainly walkoff losses, increase for high F. With an etalon tilt angle of 1 deg, a formula derived by Leeb[40] yields a round-trip power loss of 5% for the etalon in the subcavity SG, and a loss of 8% for the etalon in SL. The measured values are approximately 2 to 3 times higher. Most important, however, is that the maximum transmissible power through the etalon without damage decreases for increasing F. For example, with $F=6$ the intensity within the etalon is about 8 times higher than outside. For $F=14$ the intensity is 18 times higher.[34]

Our practical experience with the two etalons described in Table 2 shows that the frequency resolution, which is given by the ratio FSR/F, should not exceed 6 times the longitudinal-mode distance, assuming that the mirror M3 has a reflectivity $R_3\approx40\%$. As the laser pulse passes through the etalon several times during its buildup, the actual frequency resolution of the etalon is increased and the suggested frequency resolution is sufficient to discriminate against two adjacent modes. For higher values of R_3 better frequency resolution is needed.

3.3 *The Amplifier*

Here we give a brief summary of the main properties of our high-pressure amplifier, as a detailed description has been published elsewhere.[8] The laser tube has an inner diameter of 50 mm and is manufactured from Macrolon®, which is an optically transparent polycarbonate. Both ends are sealed

with a ZnSe Brewster window of 6-mm thickness. The main electrodes, with a length of 0.37 m, are made of brass. They have an Ernst profile[4] with an electrode spacing of 10 mm. The high voltage is generated by a two-stage *LC* inversion circuit.[42] The total capacitance of the main discharge circuit is 98.8 nF. The voltage across the electrodes is typically between 80 and 90 kV. In general we use a premixed laser gas of 5 : 5 : 90 CO_2 : N_2 : He at a typical flow rate of 0.5 to 1 1/min and a pressure between 11 and 11.5 bar. At higher pressures the amplification factor of our system declines dramatically and the discharge becomes unstable. The repetition rate is limited to about 0.3 Hz, because the amplifier starts arcing at higher rates.

The preionization is achieved by two preionizer rods with sliding spark arrays, which are fired about 100 ns before the main discharge. Proper alignment of the rods relative to the electrodes is imperative for arc-free operation. The best discharge stability has been achieved with following preionizer rods of new design. Each rod consists of 21 brass tubes with a length of 18 mm, which are glued on a 5-mm-diam quartz-glass tube at a distance of 7 mm. Then, a nickel wire with 1.5-mm diam is soldered on the brass tubes parallel to the quartz tube. In the last step 1-mm-wide gaps are cut perpendicular through the wire by a computer-controlled eroding machine. This guarantees exact positioning of each spark along the quartz tubes. Contrary to the usual sliding spark arrays,[43,8] this type has no sharp electrode tips at the gap, which erode easily. Nevertheless, the gap distance of the sparks increases slowly during operation, and the edges at the gaps become rounded. After approximately 250 h of operation arcing of the main discharge started to occur frequently and the spark arrays had to be replaced.

3.4 *Characteristics of the Single-Mode High-Pressure CO_2 Laser*

This section deals with the experimental characteristics of our single-mode laser system. For the detection of the laser pulses we use a photon-drag detector PDM-2 made by Edinburgh Instruments or a pyroelectric detector P5-00 manufactured by Molectron. The signals are recorded with a 750-MHz-bandwidth Tektronix 7912 HB transient digitizer or with a 500-MHz-bandwidth Tektronix TDS 620 digital oscilloscope.

In Fig. 9 we show four laser pulses, which have been produced with subcavity SG and a 70% reflectivity of the outcoupling mirror M1. The grating has been tuned to the 10P(22) transition of CO_2 at a wavelength of 10.61 μm. The laser-gas pressure was 11.0 bar. In Fig. 9(a) we present a smooth single-mode pulse with a pulse energy of about 90 mJ. When the total cavity length is changed by about one-fourth with the piezoelectric element P I (Fig. 6), mode beating of two neighboring modes occurs, as shown in Fig. 9(b). Due to slow pressure variations in the laser tube, which alter the optical length of the cavity, reliable single-mode operation is only achieved during several minutes, after which the cavity length has to be readjusted.

The pulse duration of the single-mode pulses depends strongly on the amplification factor of our oscillator. This can be easily demonstrated by measuring the pulse duration as a function of the pulse energy E. By increasing the voltage applied to the electrodes and keeping all other parameters

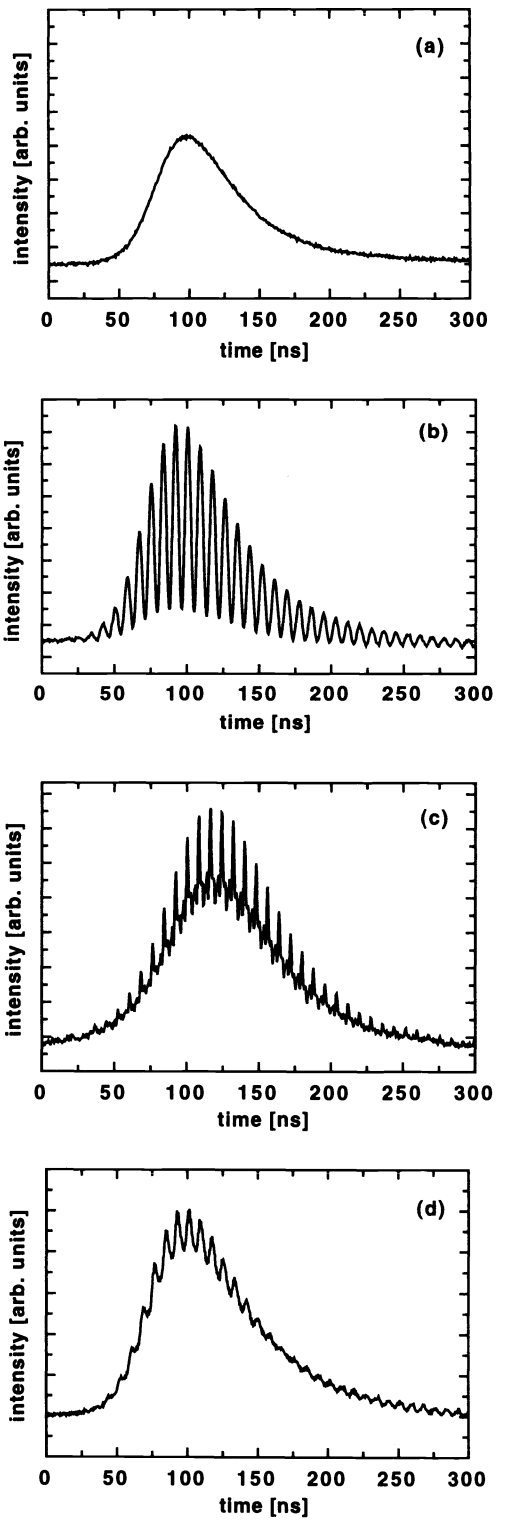

Fig. 9 Temporal shape of high-pressure CO_2 laser pulses at 10.61 μm: (a) single-mode pulse, (b) two-mode beating, (c) parasitic modes due to the 10P(20) transition, (d) three-mirror resonator without etalon.

fixed, the following FWHM pulse duration Δt is observed: $\Delta t = 130$ ns for $E = 30$ mJ, $\Delta t = 80$ ns for $E = 50$ mJ, and $\Delta t = 70$ ns for $E = 65$ mJ.

The adjustment of the etalon is not critical, although lasing between the outcoupler M1 and the etalon surfaces has to be

avoided. Therefore, we used a tilt angle between 1 and 2 deg. Although the etalon was rotated perpendicular to the rotation plane of the grating, the introduction of the etalon changed the frequency selected by the grating up to 25 GHz. Due to the walkoff losses, the tilted etalon introduces an asymmetry into the resonator, which degrades the transverse mode structure. By readjusting the grating or the mirror M2 this asymmetry can be partially compensated and a pattern similar to a TEM_{00} mode obtained.

In the situation illustrated by Fig. 9(c) the laser beam between the etalon and the mirror M3 was blocked, so that the resonator consisted effectively of the two mirrors M1 and M3 alone. In this case a high amplification factor is needed to reach the lasing threshold, because the two mirrors correspond to a single output coupler with a reflectivity of only 20%. The pulse is strongly structured by self-mode-locking.[44] The measured wavelength is about 10.6 μm, which corresponds to the 10P(20) CO_2 laser transition. At a laser gas pressure of 11 bar there exist several transitions of nearly equal strength,[3] but the 10P(20) line is favored by the optical coatings. The lasing threshold mentioned determines the maximal possible amplification factor that can be used with the three-mirror resonator to prevent parasitic oscillations on the 10P(20) line.

When the resonator is applied without the etalon, a conventional three-mirror resonator is obtained.[21] The considerable reduction of the number of simultaneously oscillating modes is easily recognized in Fig. 9(d). Nevertheless, it was not possible to produce single-mode pulses with this arrangement.

In Fig. 10 the tuning characteristics of our laser at 11.1 bar for the R and P bands at 10.4 μm are presented. All parameters of the amplifier were kept fixed during the measurement, and the single-mode pulse energy was averaged over five pulses at each grating position. In the 9.4-μm band the laser was continuously tunable in the R branch from R 12 to R 22, but not in the P branch, where lasing was only possible at the line centers.

The frequency tuning ranges of the two subcavities are quite similar. However, the reflectivity of our etalon surfaces and therefore the frequency resolution depend strongly on the wavelength. For example one of the etalons has a reflectivity of 80% at 10.6 μm, whereas at 9.4 μm it is only 75%. This causes a reduction of the finesse from 14 to 10. The effect is especially strong for the high-finesse etalon of the subcavity SL. Therefore, the reflectivity of the mirror M3 has to be reduced from 50% to 40%, when SL is operated at 9.5 μm instead of 10.5 μm. Even then, the single-mode operation stability of SG is better than that of SL in the 9.4-μm band. In the 10.4-μm band there are practically no differences.

A smooth pulse such as that shown in Fig. 9(a) is not sufficient to prove the existence of a single longitudinal mode. It is still possible that there exist additional modes separated by the FSR of the etalon, i.e., 3 or 6 GHz, or the parasitic oscillations on the 10P(20) line mentioned before. The resulting high beat frequency cannot be observed on the oscilloscope, because of the limited bandwidth. In order to detect these hidden modes we use the following procedure. A smooth pulse, which appears as a single-mode pulse on a 750-MHz oscilloscope, is passed through an absorber with an attenuation factor of at least $10^4$and a spectral width below

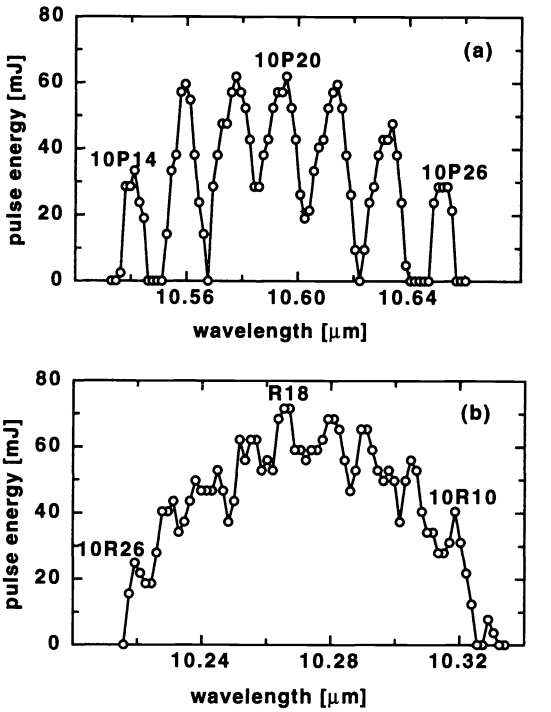

Fig. 10 Tuning characteristics at 11.1 bar for the *P* band (a) and the *R* band (b) of the 10.4-μm branch. The subcavity SG was used.

1 GHz. The laser frequency is tuned to the absorbing transition, and the ratio Q of the initial intensity I_{init} versus the attenuated intensity I_{att} is measured. The absorber suppresses the intensity I_{single} of the single-mode part nearly completely, but leaves possible existing side modes unaffected. Therefore the ratio Q can be written as

$$Q=\frac{I_{\text{init}}}{I_{\text{att}}}=\frac{I_{\text{init}}}{I_{\text{init}}-I_{\text{single}}} \quad . \tag{7}$$

A high Q indicates that the hidden modes are weak. For example, if $Q=100$, then 99% of the total laser intensity is in a single longitudinal mode, provided that no beating is observed on the oscilloscope. The quantity Q can be regarded as a quality factor, because it describes the purity of the single-mode pulse.

In the experiment we employed the subcavity SL with $L_{\text{sub}}\approx 92$ mm and various gaseous absorbers in a cell of 6-m length. Then the laser frequency was tuned onto a strongly absorbing transition, and a smooth pulse was passed through the cell. By varying the temperature of the etalon and with the piezoelectric element P II, the maximal Q factor was determined with the help of two pyroelectric detectors. The measured Q factors and other main parameters of the experiment are listed in Table 3. At all investigated wavelengths, even 16 Ghz off the CO_2 line center, we achieved a Q factor of at least 200. However, L_{sub} has to be well adjusted, as will be discussed in the next paragraph. The wavelength dependence of Q is due to the frequency-dependent amplification factor of the laser. The value of Q decreases rather rapidly at higher pulse energies because of the parasitic 10P(20) mode.

Table 3 Overview of the absorbing transitions used to investigate the mode discrimination of the laser (Q factor) as well as to generate OFID pulses (Sec. 4.1).

absorber gas molecule	CO_2 [700K]	NH_3	NH_3	NH_3	D_20
wavelength of absorption line	10,59 μm	10.55 μm	10.29 μm	9.30 μm	9.26 μm
offset from nearest CO_2 line [GHz]	0	14.6	-1.45	16.7	-0.33
single-mode pulse energy [mJ]	90	35	50	40	60
Q factor (see chap. 3.4)	≈ 1800	≈ 275	≈ 350	≈ 200	≈ 400
absorber gas transition	10P20	sP(1,0)	aR(1,1)	aR(6,2)	(4,2,2) →(5,3,3)
pressure in gas cell	250 mbar	15 mbar	10 mbar	10 mbar	10 mbar

The adjustment of the subcavity length L_{sub} is divided into two parts: a coarse tuning in the millimeter range and a fine tuning in the micrometer range. First we discuss the fine tuning between 0 and 10 μm, which is achieved with the piezoelectric element P II (Fig. 6). The experiment is similar to the preceding one. A laser pulse is transmitted through a 3.5-m-long gas cell, which is filled with 5 mbar of D_2O. The absorbing transition of D_2O at 9.26 μm is detected via a photoacoustic signal. This signal is produced by a microphone, which is incorporated into the gas cell. Then, the output energy of the laser and the photoacoustic signal are simultaneously recorded as a function of the voltage applied to the piezoelectric element P II. The result of the measurement is shown in Fig. 11. The strong modulation of the photoacoustic signal indicates that the laser frequency is a function of L_{sub}. The modulation of the pulse energy is less strong, but also clearly visible. The distance between the peaks in the diagram corresponds to a subcavity length shift of about $\lambda/2$.

Secondly, we consider the coarse adjustment of L_{sub}. The aim is to determine the L_{sub} that provides the best mode discrimination. In the experiment we measured the Q factor as a function of L_{sub}, which we varied in steps of 1 to 3 mm by moving the mirror M3. The maximum Q factor is determined at each position by fine tuning $L_{sub}$with P II. The result of such a measurement is shown in Fig. 12. For this measurement we have taken the absorbing transition sP(1,0) of NH_3 at a pressure of 16 mbar. The laser was operated with the subcavity SL at 10.55 μm. The diagram indicates clearly the region where the Q factor is maximal, i.e., where the mode discrimination as defined in Sec. 2.2 has a maximum. The measured L_{sub} at the maximum of Q is $L_{sub} = 92 \pm 2$ mm. This is in good agreement with the theoretical value of 94 mm, which is given by Eq. (6).

Apart from the specific resonator configuration, the maximal single-mode pulse energy depends strongly on the degree of destruction of the etalon and the parasitic modes at 10.59 μm tolerated. For example, at 10.59 μm [10P(20)] with the subcavity SL and an M3 with $R_3 = 40\%$, a surface plasma was generated on the etalon at pulse energies above 100 mJ, while with $R_3 = 50\%$ pulse energies of up to 120 mJ were possible. With the same configuration at 10.55 μm, 15 GHz off the 10P(16) transition of CO_2 (Table 3), we have achieved a maximum pulse energy of 95 mJ with $R_3 = 40\%$. With $R_3 = 50\%$ the amplification factor had to be reduced considerably to prevent oscillation on the 10P(20) mode, and

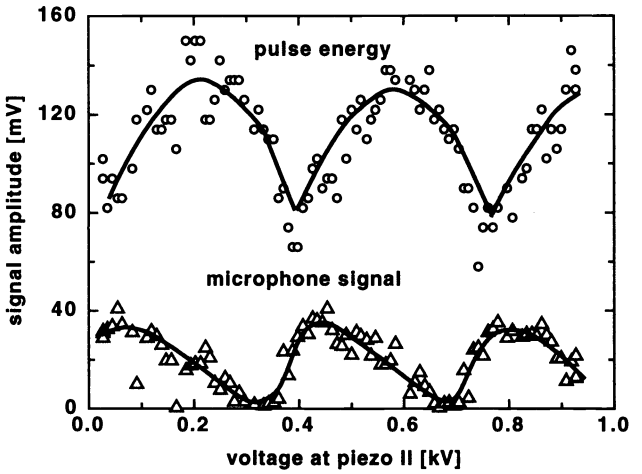

Fig. 11 Influence of the subcavity length L_{sub} tuned with the piezoelectric element P II on pulse energy (○) and photoacoustic signal (△). The photoacoustic signal indicates that the laser frequency is not permanently situated on the absorbing transition.

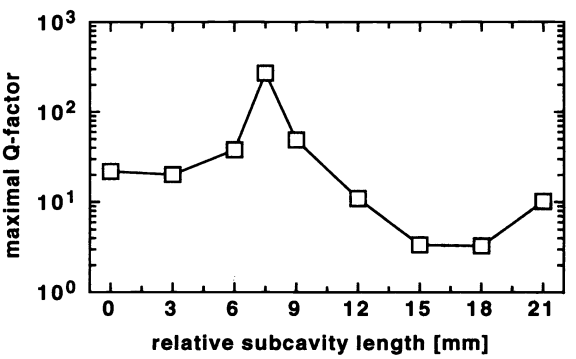

Fig. 12 The subcavity length L_{sub} influences the mode discrimination ratio, which is described by the Q factor.

the pulse energy amounted to about 30 to 40 mJ. Especially with the subcavity SL, the maximal pulse energy is not determined by the amplifier. At the strong CO_2 laser lines, the pulse energy is limited by the damage threshold of the etalon, whereas at weak lines, or in between lines, the energy is limited by parasitic oscillations of the 10P(20) transition. The losses in the subcavity SG are approximately 35% higher than in SL, because the 30% reflection loss of the grating at grazing incidence[38] is not totally compensated by the low-finesse etalon. Therefore, high amplification factors are needed, and the parasitic 10P(20) transition is especially disturbing. This problem can be reduced with a smoother amplification profile, i.e., a higher laser-gas pressure.

Finally, we summarize the particular advantages of each subcavity. The advantages of SL are the simpler grating arrangement, the larger tuning range of the etalon, a better transverse mode pattern, and a shorter total length. As the radiation losses are relatively small, higher pulse energies are possible on weak lines. On the contrary, subcavity SG shows better performance in the 9.4-μm band. Most important is that the low-finesse etalon of SG is less sensitive to destruction. Thus, pulse energies of up to 140 mJ can be obtained without damaging the etalon.

3.5 *Tunable Truncated CO_2 Laser Pulses*

In the introduction we mentioned the suitability of truncated CO_2 laser pulses for the generation of short pulses in the infrared and in the FIR region. Quite generally the rapid decay of a truncated laser pulse permits the observation of the post-pulse development in an experiment, which would otherwise be disturbed by the slowly decaying rear part of the pulse. This makes truncated pulses interesting for applications such as detector tests and for material characterization by photoacoustically induced surface displacements.

Truncated CO_2 laser pulses are produced with a plasma shutter. The laser beam itself generates a plasma by laser-induced gas breakdown at the center of a telescope. When the plasma reaches a certain electron density, the laser radiation is blocked. Due to the rapid expansion of the plasma, which can be as fast[45] as 2×10^6 m/s, truncation times of 10 ps are possible.[31]

The tunability of our single-mode laser allows the generation of frequency-tunable truncated laser pulses. In order to generate these pulses we have coupled our single-mode laser to a plasma shutter. The setup is shown in Fig. 13. The plasma shutter consists of a 1 : 1 telescope formed by two ZnSe lenses with 1-in. focal length. The lenses are housed in a metal cell, which is flushed with air at a typical pressure of 100 mbar. Two translation stages and a gimbal mount permit precise positioning of the cell. Usually the gas pressure is chosen slightly below self-breakdown of the laser radiation. The plasma breakdown is initiated by a high-voltage discharge, which provides the starting free electrons in the focus of the telescope. The high voltage is generated by a simple pulse-forming network, which is triggered by the CO_2 laser via a laser-triggered spark gap (LTSG). Finally, the divergence of the truncated pulse can be manipulated by changing the length of the telescope.

Truncated CO_2 laser pulses are shown in Fig. 14 and Fig. 18(a). More details are given in the next section, where truncated pulses are applied in various experiments.

4 Applications

4.1 *The Generation of Short Infrared Pulses by OFID*

Optical free induction decay (OFID), which is the optical analog to free induction decay in nuclear magnetic resonance,[46] is a simple pulse-shaping technique to generate single 10-μm pulses of a duration between 30 and 200 ps. In spite of the low efficiency (less than 0.1% of the initial pulse energy) and the peculiar frequency spectrum of the pulse,[47] the lack of alternative techniques makes this method attractive. Current applications are, e.g., the test of infrared detectors and the investigation of high-T_c superconductors.[48]

The basic concept of OFID, which was first realized by Yablonovitch et al.,[49] is the following: A smooth CO_2 laser pulse is abruptly truncated within 10 ps by a plasma shutter. Due to this fast truncation, large frequency sidebands (as wide as 100 GHz) are generated. By passing the truncated pulse through a spectral filter, which completely suppresses the laser frequency but leaves the sidebands unaffected, a pico-

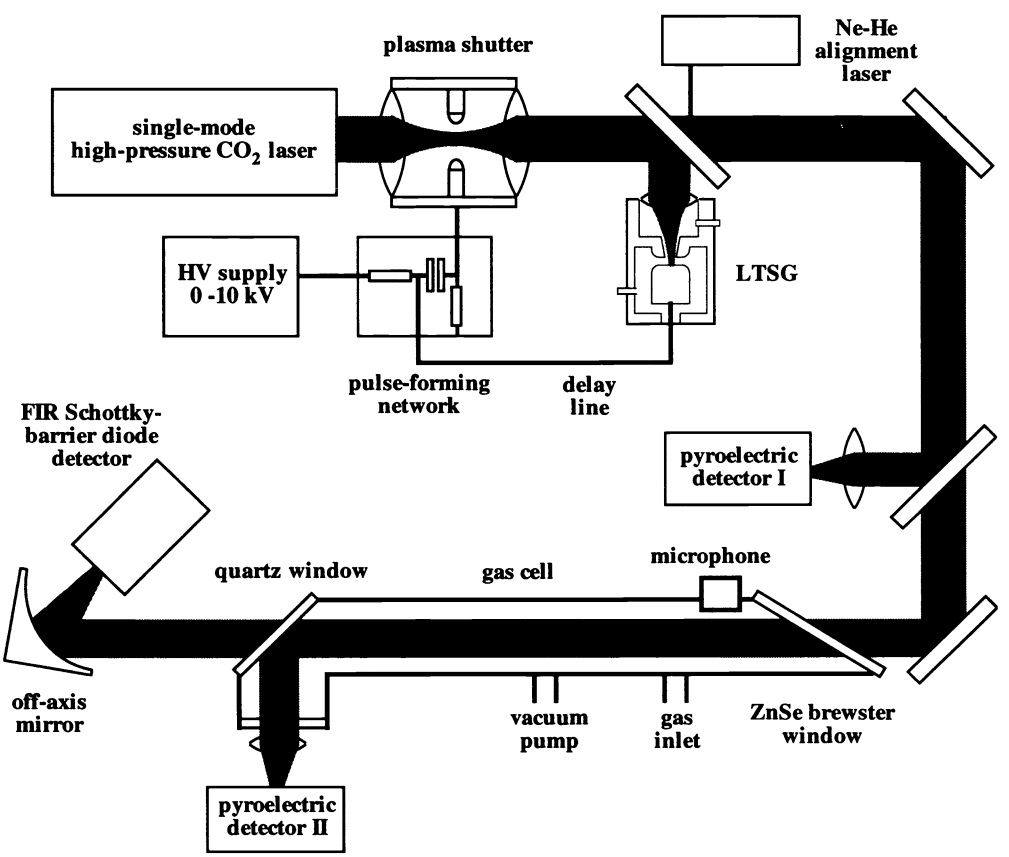

Fig. 13 Experimental setup for the generation and application of tunable truncated CO_2 laser pulses.

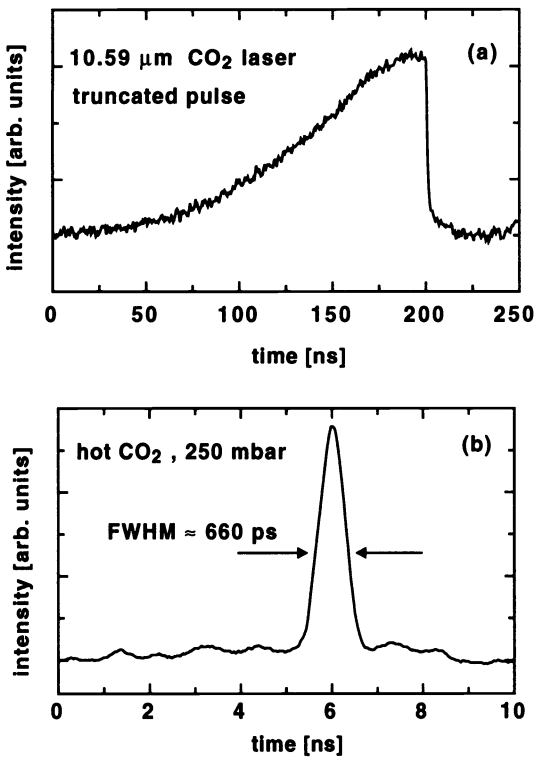

Fig. 14 Generation of 100-ps pulses by OFID: (a) truncated 10.59-μm pulse, (b) 10.59-μm OFID pulse.

second pulse is formed. With a theory based on linear-system analysis in the frequency domain and assuming that the cutoff of the laser beam has the form of a falling step function, Yablonovitch et al.[49] obtained an analytical function for the OFID pulse. In this case the OFID pulse duration t_{OFID} is given by

$$t_{OFID} = \frac{T_2}{\alpha L} , \tag{8}$$

where αL is the absorption length in nepers (Np) and T_2 the transverse relaxation time of the absorber molecules.

In standard OFID systems, which work with TEA CO_2 lasers, hot CO_2 gas[50] has mainly been used as spectral filter. Recently Scherrer and Kneubühl[5] discovered that FIR laser gases, such as D_2O, NH_3, or CH_3F, could be applied as well. These gases are easier to handle than hot CO_2, because no additional heating device is required, and shorter gas cells with low pressure can be employed due to the high absorption coefficient of FIR laser gases. However, coincidence of the CO_2 laser frequency and the absorbing transition is no longer achieved automatically. This problem can be circumvented with a tunable CO_2 laser system, which produces ultrashort OFID pulses at numerous frequencies. Furthermore, the gain-switched pulses of the high-pressure CO_2 laser are advantageous over the relatively long TEA CO_2 laser pulses, because the OFID pulse energy depends on the peak power of the laser pulse and not on the total energy.

The experimental setup of our OFID system is shown in Fig. 13. After leaving the plasma shutter, the truncated laser pulse is passed through a gas cell with variable length, which contains the spectral filter. Two pyroelectric detectors (P5-00) monitor the entering and the transmitted CO_2 laser pulse. Their signals are recorded by a fast oscilloscope (see Sec. 3.5). The signal of the transmitted laser pulse is amplified by a factor of 10 with a 1-GHz-bandwidth preamplifier.

To make sure that our OFID system works, we started with the usual hot CO_2 gas as spectral filter. The laser beam was passed two times through a 3-m-long glass tube, whose temperature was automatically kept at about 670 K. This so-called "hot cell" was connected to a vacuum system and equipped with NaCl Brewster windows.[31] Using the sub-cavity SL, the laser was tuned to the wavelength 10.59 μm of the 10P(20) transition. The pulse energy was 120 mJ before entering the plasma shutter and 60 mJ after being truncated. A truncated laser pulse is shown in Fig. 14(a). When the hot cell was filled with 250 mbar of CO_2, OFID pulses like that shown in Fig. 14(b) were obtained. The pulse had an apparent duration of about 660 ps, which is determined by the limited bandwidth of our detection system. The true duration, which is[45] about 50 ps, can be determined by autocorrelation measurements.[8]

Next, we investigated the influence of a frequency offset $\Delta\nu$ between the laser line and the absorption line of the spectral filter. Figure 15(a) shows an OFID pulse at 10.61 μm. The spectral filter was the 10P(22) transition of hot CO_2 gas at 130 mbar. By changing the temperature of the etalon by 0.25 K, the laser frequency is shifted by about 250 MHz and consequently the absorption coefficient at the laser frequency declines. This is shown in Fig. 15(b), where the OFID pulse is preceded by a pretail of the truncated laser pulse, which is no longer completely absorbed. When the pressure of the hot CO_2 gas is increased to 340 mbar, the absorbing transition is pressure broadened from a FWHM of 0.5 GHz to 1.3 GHz. This increases the absorption at $\Delta\nu = 250$ MHz, and an OFID pulse without pretail reappears again [Fig. 15(c)]. Simultaneously, the pulse energy decreases by a factor of about 7. At $\Delta\nu$ of 450 MHz a CO_2 pressure of 430 mbar is needed to suppress the pretail, and the pulse energy is about 18 times lower than at 120 mbar. The frequency spectrum of the OFID pulse is asymmetric if $\Delta\nu \neq 0$. This is shown in Fig. 16, where we have plotted the calculated spectral intensity of the OFID pulse corresponding to the pulses shown in Fig. 15(a) and 15(c). As the frequency shift barely affects the large frequency sidebands, the OFID pulse is not strongly affected, and so the pulse in Fig. 15(c) corresponds to an OFID pulse at $\Delta\nu = 0$ and $p = 340$ mbar.

A numerical calculation of the OFID pulse shape via Fourier transformation of the frequency spectrum demonstrates that an increase of $|\Delta\nu|$ is connected with an increase of peak intensity and pulse duration. This is observed in Fig. 17, where we show calculated peak intensity and duration of the OFID pulse as a function of $\Delta\nu$ for a pressure of 430 mbar in a 6-m-long cell. The temporal truncation profile of the laser pulse has been approximated[31] with an exponential E-field decay with a truncation time of about 15 ps. At $|\Delta\nu| > 500$ MHz the attenuation of the pretail is less than 50 and the energy of the pretail exceeds the energy of the OFID pulse. However, a longer gas cell or a more strongly absorbing transition would permit shifts $|\Delta\nu|$ larger than 500 MHz. This experiment demonstrates that it is possible to compensate a frequency difference of at least 500 MHz between laser and spectral filter by pressure broadening of the absorbing transition. This allows continuous frequency tuning of the OFID pulses in that region.

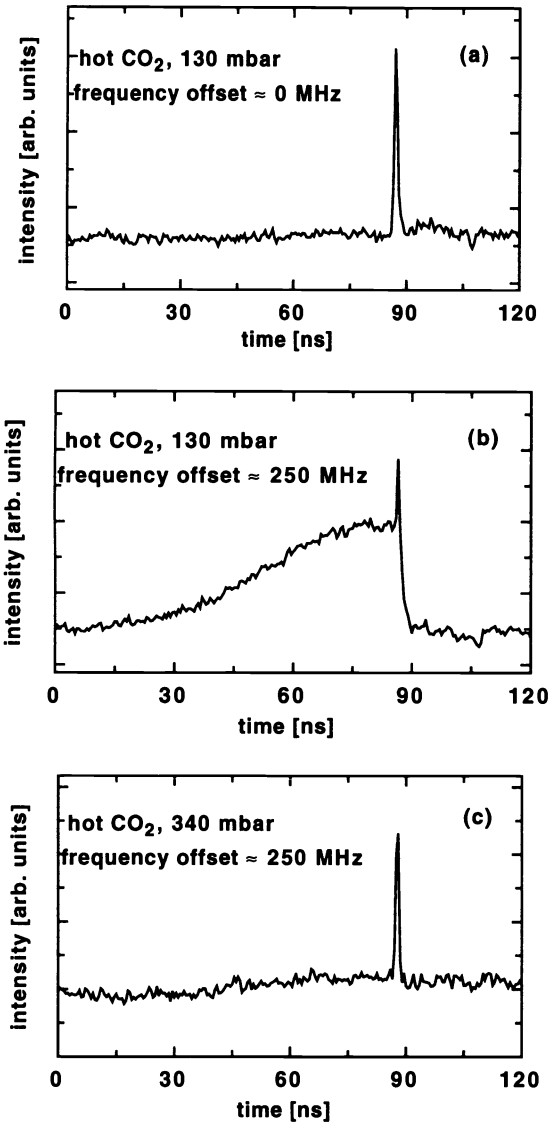

Fig. 15 Off-resonant generation of OFID pulses at 10.61 μm with hot CO_2 at pressure p: (a) $p=130$ mbar, frequency detuning from the 10P(22) CO_2 line center $\Delta\nu=0$ MHz; (b) OFID pulse with pretail at $p=130$ mbar and $\Delta\nu=250$ MHz; (c) $p=340$ mbar and $\Delta\nu=250$ MHz.

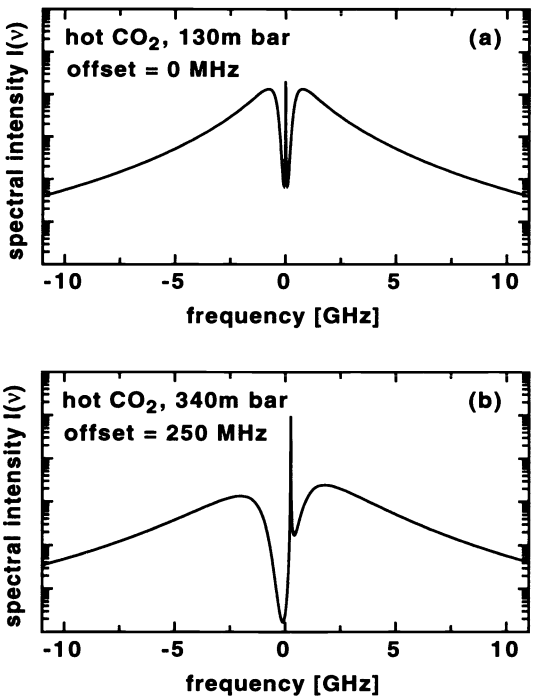

Fig. 16 Numerically calculated frequency spectrum of the OFID pulse of Fig. 15: (a) symmetric spectrum at $\Delta\nu=0$ MHz corresponding to Fig. 15(a); (b) asymmetric spectrum at $\Delta\nu=250$ MHz corresponding to Fig. 15(c).

In the following experiments we have replaced the hot cell by a glass tube of 1.3-m length and of 26-mm diam. A ZnSe Brewster window was used at the entrance, whereas a quartz window mounted at 45 deg was applied to separate the CO_2 laser radiation from FIR radiation eventually generated. A microphone, which is mounted close to the entrance of the gas cell, makes it easier to tune the laser on the desired absorption line.

In order to take advantage of the large frequency tunability of the high-pressure CO_2 laser, we have used the sP(1,0) transition of NH_3 at 10.55 μm as the spectral filter in our OFID system. This transition is situated 14.6 GHz off the 10P(16) CO_2 laser line. To achieve a high single-mode pulse energy we have chosen the subcavity SL and a reflectivity of 40% for the mirror M3. At a laser-gas pressure of 12.5 bar we have obtained pulse energies of up to 95 mJ with a transverse mode similar to a TEM_{00}. Higher pulse energies were not possible, because an optical-breakdown plasma started to form on the surfaces of the etalon. With the truncated CO_2 laser pulse shown in Fig. 18(a), we have produced the OFID pulse in Fig. 18(b). The NH_3 pressure was 38 mbar. At a pressure of 25 mbar an OFID pulse with the typical pretail is generated as shown in Fig. 18(c) an 18(d). Due to the short gas cell, saturation of the absorber gas occurred. At low intensity the pulse shape of the pretail increases gradually [Fig. 18(d)], whereas at a 2.5 times higher pulse intensity the increase is clearly enhanced [Fig. 18(c)].

A similar experiment was performed with the aR(1,1) transition of NH_3. This transition is at 10.29 μm about -1.5 GHz off the 10R(14) transition of CO_2. With a CO_2-laser pulse energy near 100 mJ and a NH_3 pressure of 12 mbar, the OFID pulses had an apparent FWHM of 720 ps. At about 9 mbar, absorption saturation effects were again clearly visible at the pretail. For a 6-m gas cell a gas pressure of about 2 mbar was sufficient to suppress the pretail. However, mid-infrared radiation, which was simultaneously generated by optically pumping the NH_3 gas via a Raman process, perturbed the measurement.

The major problem of our OFID system is the low laser-pulse energy. At low pulse energies the truncation speed of the plasma shutter is reduced,[50] and the generation of the sidebands, which constitute the OFID pulse, is less effective. Kälin et al.[31] demonstrated by theory that in this case the energy of OFID pulse strongly declines and the pulse duration increases. Therefore, we have investigated the influence of the laser-pulse energy with a standard OFID system that consists of a grating-tunable hybrid TEA CO_2 laser, a plasma shutter, which is identical to the one used in the preceding experiments, and a hot CO_2 cell.[31] The hot cell was filled

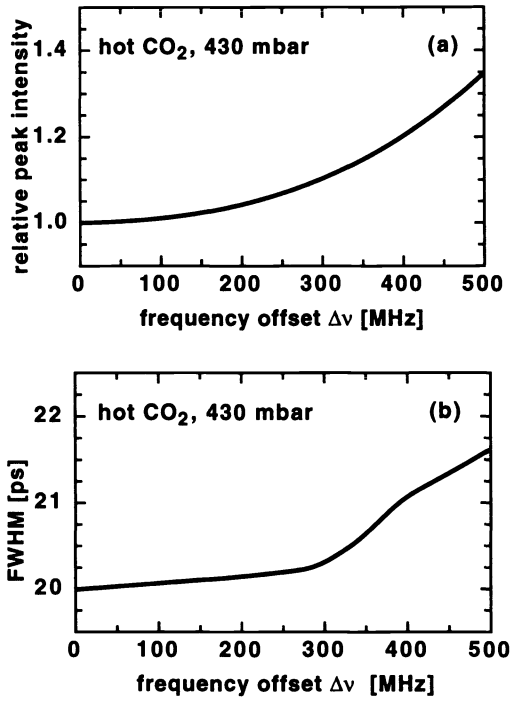

Fig. 17 Numerically calculated relative peak intensity (a) and duration (b) of OFID pulses at 430-mbar hot CO_2 versus frequency detuning $\Delta\nu$ from the absorption line center. A truncation time of 15 ps was assumed.

with 160 mbar of CO_2 gas at a temperature of 670 K. The laser was tuned to a wavelength of 10.25 μm [10R(20)]. The OFID pulses were detected with a photovoltaic GaAs–AlGaAs multi-quantum-well infrared detector, which operates without bias voltage. The detector was cooled down to liquid-nitrogen temperature. With a 200-mJ laser pulse we produced the OFID pulse in Fig. 19(a). Again the apparent pulse duration is mainly determined by the detection system, and the real FWHM is approximately 60 ps. Then an attenuator was placed between the laser and the plasma shutter, which reduced the laser energy to about 40 mJ. The apparent OFID pulse duration increased considerably, and the average pulse amplitude declined by a factor of 180, although the intensity of the truncated pulse was only decreased by a factor of 5 [Fig. 19(b)]. Furthermore, the pulses were less stable than before. When the laser pulse energy was further reduced, double pulse structures occurred frequently, as shown in Fig. 19(c). These results indicate that OFID pulse generation with our plasma shutter is possible with laser pulse energies over 50 mJ. However, the system works reliably only with pulse energies in excess of 100 mJ. One possible method to produce OFID pulses with low laser-pulse energies may be the use of a telescope in the plasma shutter with a focal length below 1 in. to increase the radiation intensity in the focus (Sec. 3.5).

4.2 *The Generation of Superradiant FIR Pulses*

Here we demonstrate the use of our laser system for the generation of single FIR pulses by superradiance in a gaseous medium.

Superradiance is a quantum-mechanical process, which is based on coherent spontaneous emission arising from many atoms that are emitting collectively.[32,52] Due to the mutual

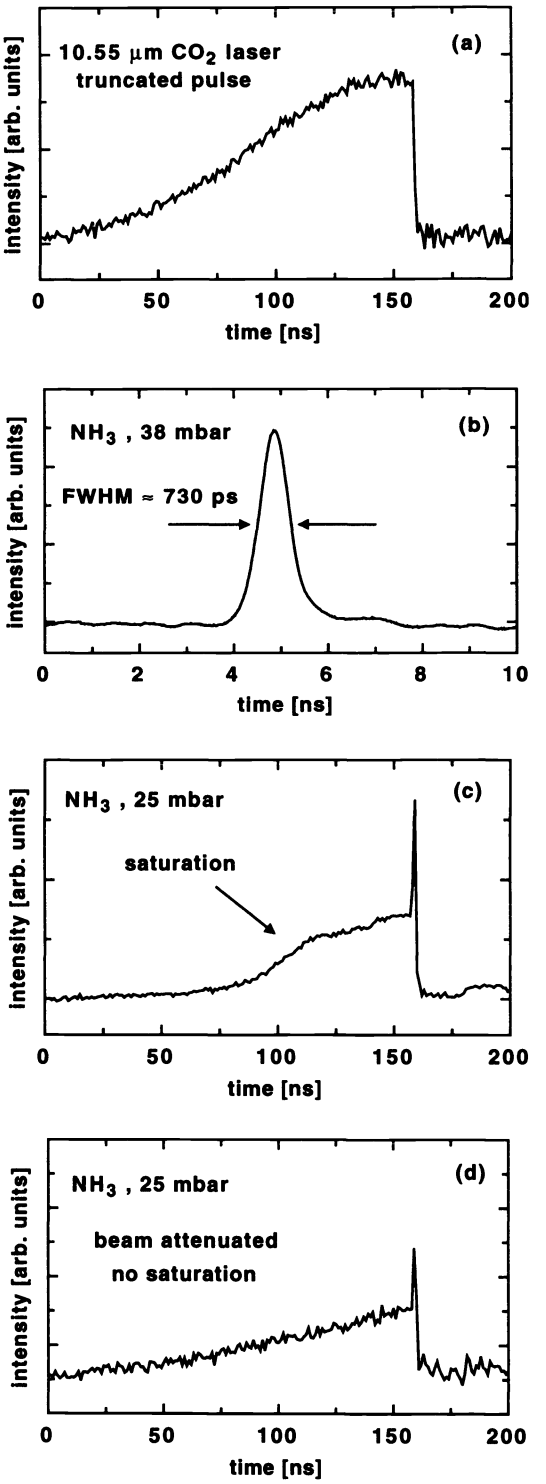

Fig. 18 OFID pulses generated with NH_3 14.6 GHz off the 10P(16) CO_2 laser line center: (a) truncated 10.55-μm CO_2 laser pulse; (b) OFID pulse for an NH_3 pressure $p=38$ mbar; (c) OFID pulse with pretail for $p=25$ mbar (the pretail is deformed by saturation effects in the absorber); (d) same as in (c) except that the intensity of the truncated pulse is reduced to 40%.

interaction of the optically excited gas atoms, the decay time of the excited levels is considerably decreased and single short FIR pulses are produced. For example, Scherrer et al.[53] generated 800-ps, 291-μm pulses with NH_3. Superradiant

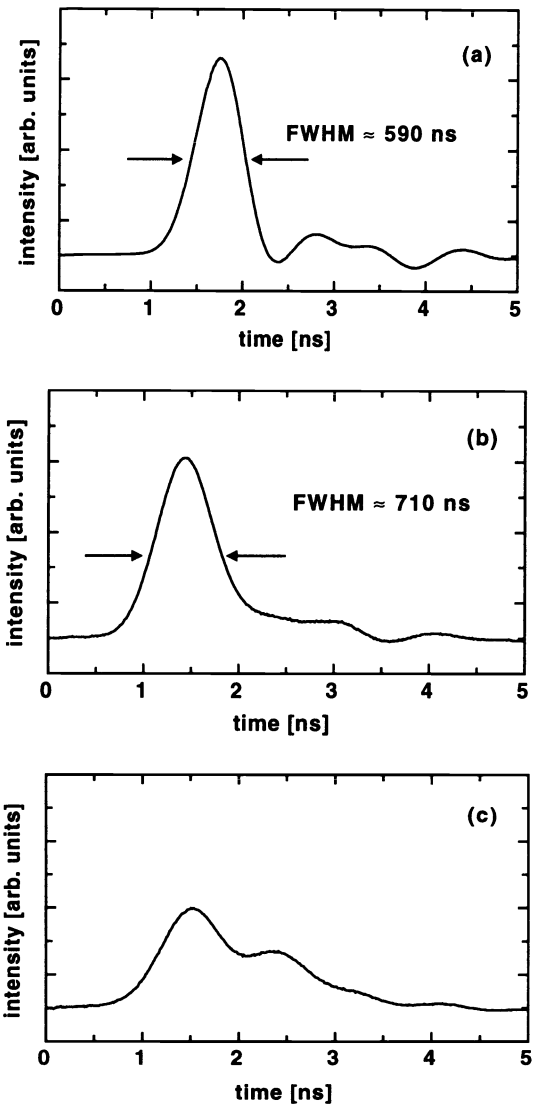

Fig. 19 Influence of the 10.25-μm CO_2 laser-pulse energy prior to the truncation on the apparent OFID pulse duration for a pulse energy of (a) 200 mJ; (b) 40 mJ; (c)≈30 mJ (a broad double pulse appears). The filter is hot CO_2.

pulses show the following characteristic features: a delay Δt relative to the pump pulse with $\Delta t \propto 1/N$, a pulse duration $t_p \propto 1/N$, and a peak intensity $I \propto N^2$, where N is the number of emitting molecules. It should be noticed that superradiance has to be distinguished from the process of amplified spontaneous emission, which is observed in many so-called "mirrorless lasers."[54]

The use of truncated CO_2 laser pulses to pump superradiant laser systems has several advantages. First, the pump pulses are smooth, which avoids the generation of Raman radiation at intensity spikes. Secondly, these pump pulses have a well-defined temporal duration after which the superradiant system is no more influenced by the pump pulse. Furthermore, the frequency broadening of the pump pulse, which is caused by the fast truncation process, permits the generation of even shorter FIR pulses with certain pump media.[32]

Variations of the pump-laser frequency have no influence on the frequency of the FIR radiation, which depends only on the excited-molecule transition. However, it influences the total energy that is absorbed by the FIR medium.

In this experiment we have pumped the well-known line of D_2O at 9.26 μm, which lies 320 MHz off the 9R(22) transition of CO_2 . The experimental setup, which is identical to that used in Sec. 4.1, is shown in Fig. 13. After the generation of a truncated 9.26-μm laser pulse, which had an energy of about 30 mJ, the pulse was sent through a 3.5-m gas cell. The generated FIR radiation was detected with a fast and sensitive Schottky-barrier diode.[55] In Fig. 20(b) a superradiant 385-μm FIR pulse is shown, which was pumped by the truncated laser pulse of Fig. 20(a). This pulse has been generated at a pressure of 0.12 mbar. It shows the typical delay Δt relative to the 9.26-μm pump pulse, which was 34 ns in this experiment. By increasing the gas pressure $p \propto N$ the delay Δt and the pulse duration decreased, whereas the FIR pulse energy increased. Subsequently, we tried to generate superradiant FIR radiation with D_2O at the pump frequencies[56] of 9.275, 9.295, and 9.298 μm. With these transitions we have observed FIR radiation generated via the Raman process,[10] but no superradiant radiation. However, we do not know whether it is possible at all to produce superradiant FIR radiation on these transitions. This is difficult to predict, because molecular transitions of superradiant lasers have to fulfill several conditions.[57]

5 Conclusions

We have developed a single-mode high-pressure CO_2 laser system. Single-longitudinal-mode operation has been achieved with a three-mirror resonator with etalon. In particular we have investigated two resonator configurations: The first included a grating in Littrow arrangement and an

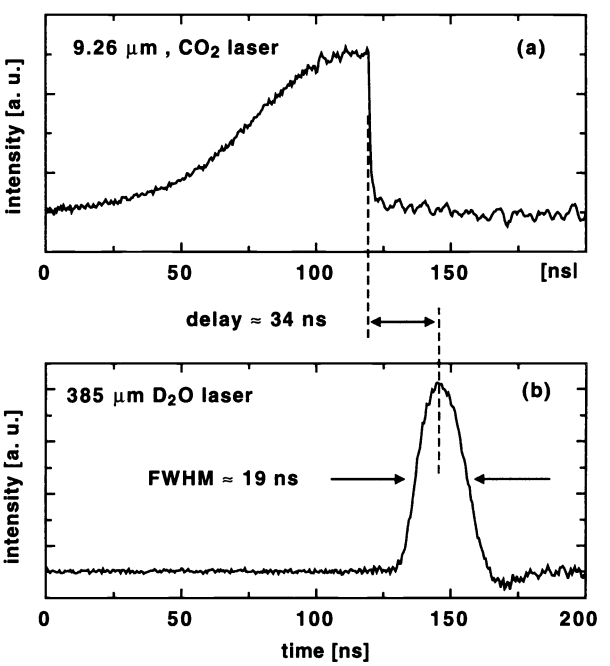

Fig. 20 Generation of superradiant FIR pulses at 385 μm: (a) truncated 9.26-μm CO_2 pump pulse, (b) 19-ns superradiant FIR pulse at a D_2O pressure of 0.12 mbar.

etalon with a finesse of 14. In the second configuration the grating was employed in grazing incidence, which allowed the use of an etalon with a finesse of only 6. The first arrangement proved to be better suited for single-mode operation on weak transitions, while the second permitted 20% higher pulse energies of up to 140 mJ without damaging the etalon.

Furthermore, a theoretical model of the resonator has been developed, which illustrates its frequency-tuning behavior. Theory and experiment demonstrate the relevance of the subcavity length to achieve the best possible mode discrimination of the resonator.

In combination with a plasma shutter, the laser system has been applied to generate frequency tunable, truncated laser pulses. These pulses have been used in an OFID system. For the first time 100-ps OFID laser pulses have been generated with a tunable high-pressure CO_2 laser. Thus we produced, e.g., OFID pulses 15 GHz off the 10P(16) CO_2-laser line center at 10.55 μm with NH_3 gas as the spectral filter. In addition, we have produced frequency-tunable OFID pulses in a range of about ±500 MHz at the absorbing transition of the spectral filter by pressure broadening of the transition. Finally, our truncated CO_2 laser pulses have been used to generate 385-μm FIR superradiant pulses to demonstrate a further application of our laser system.

Acknowledgments

We wish to thank Professor J. R. Izatt, University of Alabama, Tuscalosa, USA, Dr. L. R. Botha, Atomic Energy Corporation of South-Africa, Pretoria, and Dr. A. W. Kälin Spiez, Switzerland, for suggestions and discussions.

This study was supported by the Swiss National Science Foundation, the GRD/EMD Bern and the ETH Zürich.

References

1. A. J. Alcock, K. Leopold, and M. C. Richardson, "Continuously tunable high-pressure CO_2 laser with UV photopreionization," *Appl. Phys. Lett.* **23,** 562–564 (1973).
2. V. N. Bagratashvili, I. N. Knyazev, V. S. Kudryavtsey, and V. S. Letokhov, "Frequency tuning of an e-beam preionized high-pressure CO_2 laser," *Opt. Comm.* **9,** 135–138 (1973).
3. S. Taylor, A. J. Alcock, W. J. Sarjeant, and K. E. Leopold, "Electrical and gain characteristics of a multi-atmosphere UV-preionized CO_2 laser," *IEEE J. Quantum Electron.* **QE-15,** 1131-1140 (1979).
4. C. Angelié, R. Capitini, and P. Girard, "Longitudinal mode selection by injection in a high-pressure CO_2 laser," *Appl. Opt.* **26,** 1074–1080 (1987).
5. A. J. Alcock and A. C. Walker, "Generation and detection of 150 psec mode-locked pulses from a multi-atmosphere CO_2 laser," *Appl. Phys. Lett.* **23,** 562–564 (1974).
6. P. T. Lang, W. Schatz, K. F. Renk, E. V. Beregulin, S. D. Ganichev, and I. D. Yaroshetskii, "Generation of far-infrared pulses by use of a passively mode-locked high-pressure CO_2 laser," *Int. J. Infrared and Millimeter Waves* **11,** 851–856 (1990).
7. P. C. Corkum, "Amplification of picosecond 10 μm pulses in multiatmosphere CO_2 lasers," *IEEE J. Quantum Electron.* **QE-21,** 216–232(1985).
8. R. Kesselring, A. W. Kälin, H. J. Schötzau, and F. K. Kneubühl, "Picosecond CO_2 laser pulse generation and amplification," *IEEE J. Quantum Electron.* **QE-29,** 997–1005 (1993).
9. B. K. Deka, P. E. Dyer, and R. J. Winfield, "Optically pumped NH_3 laser using a continuously tunable CO_2 laser," *Opt. Comm.* **33,** 206–208 (1980).
10. P. T. Lang, "Generation of tunable high power far-infrared radiation by stimulated Raman scattering in gaseous methyl halides," *Infrared Phys.* **33,** 237–262(1992).
11. M. A. Rob and J. R. Izatt, "Intermodal tuning behaviour of an etalon-tuned three-mirror TEA CO_2 laser," *IEEE J. Quantum Electron.* **QE-28,** 56–60 (1992).
12. P. Mathieu and J. R. Izatt, "Narrow-band CO_2-TEA laser for efficient FIR laser pumping," *IEEE J. Quantum Electron.* **QE-13,** 465–468 (1977).
13. J. R. Izatt, W. Schatz, and K. F. Renk, "Length and pressure dependence of the tuning spectrum produced by CH_3F double Raman laser," *Infrared Phys.* **34,** 513–523 (1993).
14. L. R. Botha, R. N. Campbell, E. Ronander, and M. M. Michaaelis, "Numerical investigation of a three-mirror resonator for a TE CO_2 laser," *Appl. Opt.* **30,** 2447–2452 (1991).
15. W. Demtröder, *Laser Spectroscopy,* 2nd corr. print., Springer Series in Chemical Physics 5, Springer-Verlag, Berlin (1982).
16. F. K. Kneubühl and M. W. Siegrist, *Laser* (in German), 3rd ed., Teubner-Verlag, Stuttgart (1991).
17. S. L. Chin, "Various techniques for producing a single longitudinal mode TEA-CO_2 laser," *Opt. & Laser Technol.* pp. 85–88 (Apr. 1980).
18. M. Quack, C. Ruede,and G. Seyfang, "Generation of shaped pulses for IR-laser chemistry," *Spectrochim. Acta* **46A,** 523–536 (1989).
19. A. Goldhalekar and E. Holzhauer, "Single longitudinal mode operation of high pressure pulsed CO_2 lasers," *Phys. Lett.* **46A,** 229–230 (1973).
20. S. Marchetti and R. Simili, "Line narrowing in a high-pressure tunable CO_2 laser," *Opt. Commun.* **94,** 541–545 (1992).
21. B. K. Deka, P. E. Dyer, and R. J. Winfield, "Single-mode operation of a continuously tunable TE CO_2 laser using a three-mirror resonator," *Opt. Commun.* **39,** 255–258 (1981).
22. B. K. Deka, M. A. Rob, and J. R. Izatt, "Mode control and high energy operation of a multi-atmosphere TE CO_2 laser using a three-mirror resonator," *Opt. Commun.* **57,** 111–115 (1986).
23. J. Knittel, D. Scherrer, and F. K. Kneubühl, "The first optical-free-induction-decay system with a continuously tunable high-pressure CO_2 laser," *Infrared Phys. Technol.* **35,** 67–71 (1994).
24. G. Kovar, D. Larouche, M. Piche, and P. A. Belanger, "Single-longitudinal-mode operation of a TEA-CO_2 laser with a modified Fabry-Perot interferometer," *Appl. Opt.* **24,** 3584–3590 (1985).
25. E. Palange and G. Salvetti, "Longitudinal-mode selectivity and perturbation sensitivity of multimirror laser cavities," *Appl. Opt.* **30,** 3821–3831 (1991).
26. G. Kovar and M. Piche, "Single longitudinal mode operation of a continuously tunable high pressure TEA-CO_2 laser," *Proc. SPIE* **663,** 79–85 (1986).
27. J. L. Lachambre, P. Lauigne, G. Otis, and M. Noel, "Injection locking and mode selection in TEA CO_2 laser oscillators," *IEEE J. Quantum Electron.* **QE-12,** 756–764 (1976).
28. A. Chandonnet and M. Piche, "Single-mode pulses from a high pressure CO_2 laser operated below emission threshold," *IEEE J. Quantum Electron.* **QE-27,** 2226–2230 (1991).
29. J. R. Izatt, M. R. Rob, and W. S. Zhu, "Two- and three-grating resonators for high-power pulsed CO_2 lasers," *Appl. Opt.* **30,** 4319–4329 (1991).
30. J. R. Izatt, University of Alabama, Tuscaloosa, USA, private communications (1993).
31. A. W. Kälin, R. Kesselring, H. Cao, and F. K. Kneubühl, "Optical free induction decay (OFID) 10 μm CO_2 laser systems," *Infrared Phys.* **33,** 73–112 (1992).
32. D. P. Scherrer and F. K. Kneubühl, "New phenomena related to pulsed FIR superradiant and Raman emission," *Infrared Phys.* **34,** 227–267 (1993).
33. I. Shoshan, N. N. Danon, and U. P. Oppenheim, "Narrowband operation of a pulsed dye laser without intracavity beam expansion," *J. Appl. Phys.* **48,** 4495–4497 (1977).
34. K. Shimoda, *Introduction to Laser Physics,* 2nd ed., Springer-Verlag, New York (1986).
35. D. N. Raouf, "UV and X-ray preionized high-pressure CO_2 laser and line narrowing for spectroscopic studies," PhD Thesis, University of Hull, UK (1987).
36. L. R. Botha, R. N.Campbell, E. Ronander, and M. M. Michaaelis, "Single longitudinal mode resonator for the lower gain lines of a high pressure CO_2 laser," *S.-Afr. J. Phys.* **14,** 64–67 (1991).
37. J. E. Bjorkholm, "Improved use of gratings in tunable lasers," *Opt. Comm.* **4,** 283–284 (1971).
38. B. K. Deka and W. Zhu, "Improved performance of a near grazing incidence grating continuously tunable CO_2-laser," *Appl. Opt.* **25,** 4218–4220 (1986).
39. R. C. Force, S. F. Ravitz, and W. B. Kendall, "Device for the precise measurement of small temperature changes," *Rev. Sci. Instrum.* **35,** 729–733 (1964).
40. W. R. Leeb, "Losses introduced by tilting intracavity etalons," *Appl. Phys.* **6,** 267–272 (1974).
41. G. J. Ernst, "Compact uniform field electrode profiles," *Opt. Commun.* **47,** 47–51 (1983).
42. G. C. Stuart, H. Houtman, and J. Meyer, "High gain, multi-atmosphere CO_2 laser amplifier," *Rev. Sci. Instrum.* **58,** 261–264 (1987).
43. B. Norris and A. L. Smith, "Operation of sliding-spark arrays for laser pre-ionization," *J. Phys. E* **10,** 551–554 (1977).
44. U. Werling, Wan Chong-Yi, and K. F. Renk, "Tuning characteristics

of a UV preionized 20-atmosphere CO_2 laser," *Int. J. Infrared and Millimeter Waves* **6,** 449–457 (1985).
45. H. S. Kwok, "Picosecond CO_2 laser pulses and their application," *Infrared Phys.* **25,** 53–59 (1985).
46. R. L. Shoemaker, "Coherent transient infrared spectroscopy," in *Laser and Coherent Spectroscopy,* J. I. Steinfeld, Ed., Plenum Press, New York (1978).
47. P. Mukherjee and H. S. Kwok, "Resonant inhomogeneous molecular absorption of ultrashort laser pulses: role of the pulse spectrum," *J. Opt. Soc. Am. B* **10,** 425–432 (1993).
48. F. K. Kneubühl, D. P. Scherrer, and D. B. Moix, "Modern aspects of far-infrared gas lasers," *Arch. Elektrotechnik* **77,** 35–40 (1994).
49. E. Yablonovitch and J. Goldhar, "Short CO_2 laser pulse generation by optical free induction decay," *Appl. Phys. Lett.* **25,** 580–582 (1974).
50. M. Sheik-bahaei and H. S. Kwok, "Characterization of a picosecond CO_2 laser system," *Appl. Opt.* **30,** 666–670 (1985).
51. D. P. Scherrer and F. K. Kneubühl, "First realization of new ps 10-μm CO_2-OFID laser systems with far-infrared laser gases as spectral filters," *Infrared Phys.* **33,** 67–70 (1992).
52. L. Allen and J. H. Eberly, *Optical Resonances and Two-Level Atoms,* Interscience Monographs and Texts in Physics and Astronomy 28, Wiley, New York (1975).
53. D. P. Scherrer, A. W. Kälin, R. Kesselring, and F. K. Kneubühl, "Generation of ultrashort far-infrared pulses optically pumped with truncated hybrid 10 μm CO_2-laser pulses," *Opt. Commun.* **87,** 249 (1992).
54. A. T. Rosenberger, "Far-infrared superradiance in methyl fluoride," PhD Thesis, University of Illinois at Urbana-Champaign (1979).
55. R. U. Titz, H. P. Röser, G. W. Schwaab, H. J. Neilson, P. A. Wood, T. W. Crowe, W. C. Peatman, J. Prince, B. S. Deaver, H. Alius, and G. Dodel, "Investigation of GaAs Schottky barrier diodes in the THz range," *Int. J. Infrared and Millimeter Waves* **11,** 809–820 (1990).
56. C. Camy-Peyret, J. M. Flaud, and A. Mahmoudi, "Line positions and intensities in the ν_2 band of D_2O improved pumped D_2O laser frequencies," *Int. J. Infrared and Millimeter Waves* **6,** 199–233 (1985).
57. J. C. MacGillivray and M. S. Feld, "Theory of superradiance in an extended, optically thick medium," *Phys. Rev. A* **14,** 1169–1189 (1976).

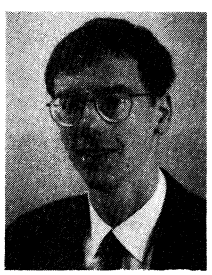

Joachim Knittel received the MS diploma in physics from the University of Konstanz, Germany, in 1989, and the PhD degree in physics from the Swiss Federal Institute of Technology, Zurich (ETH), Switzerland in 1994. Since 1995 he has been a postdoctoral research associate at the University of Zurich, where he works in the fields of nonlinear optics and molecular spectroscopy. His research interests include laser devices and nonlinear optical frequency conversion.

Damien P. Scherrer received the MS diploma in physics from the Swiss Federal Institute of Technology, Zurich (ETH), Switzerland in 1987, and the PhD degree in physics from ETH in 1992. He is currently a postdoctoral research associate in physics at the Infrared Physics Laboratory at the Institute of Quantum Electronics at ETH. His research interests include infrared and far-infrared gas lasers, optical superradiance, and related nonlinear optical phenomena.

Fritz K. Kneubühl studied physics at the Swiss Federal Institute of Technology, (ETH) Zürich and received his MS diploma in 1955 and his PhD degree in 1959. After doing research at Southampton University, UK, and Johns Hopkins University, Baltimore, USA, he returned to ETH Zürich, where he was appointed assistant professor in 1966, associate professor in 1970, and full professor in 1972. He is head of the Infrared Physics Laboratory ETH, which is involved in research on infrared physics and technology, such as quantum electronics, spectroscopy, detector development, atmospheric physics, and astrophysics. He has published several books and about 400 papers, and presided over the Quantum Electronics Division of EPS from 1976 to 1978 and the International Infrared Physics Conferences CIRP 1 to 6 in Switzerland from 1975 to 1994. He has received scientific awards in the USA, the UK, Germany, and Hungary. He is also editor in chief of *Infrared Physics & Technology* (Elsevier Science).